Exclusive vector-meson production in muon-proton scattering

C. del Papa,* D. Dorfan, S. M. Flatté, A. Grillo, C. A. Heusch, B. Lieberman,† L. Moss,‡ T. Schalk, and A. Seiden
University of California, Santa Cruz, California

K. Bunnell, M. Duong-van,§ R. Mozley, A. Odian, F. Villa, and L. C. Wang‖
Stanford Linear Accelerator Center, Stanford, California

(Received 13 July 1978)

From a muon-proton scattering experiment with a streamer chamber at the Stanford Linear Accelerator we present results in the ranges $0.3 < Q^2 < 4.7$ GeV^2 and $1.7 < W < 4.7$ GeV for the reactions $\mu^+ p \to \mu p V$ where V is a vector meson (ρ^0, ω, or ϕ). It is shown that in ρ production the skewing parameter and the longitudinal-transverse ratio change significantly as Q^2 increases above 1 GeV^2. The cross section for ρ^0 production as a function of Q^2 falls below the vector-meson-dominance prediction. The ratio of the cross section for exclusive vector-meson production to the total cross section falls by a factor of 10 between photoproduction and a Q^2 of 2 GeV^2, yet the ratio of ω to ρ production remains constant at the photoproduction value out to $Q^2 > 2$ GeV^2.

I. INTRODUCTION

A. Theoretical background

The idea that the photon-hadron coupling occurs primarily through the vector mesons (vector-meson dominance or VMD) has had remarkable success in quantitatively explaining the behavior of the interaction of real photons with nucleons, including the total γN cross section, vector-meson production and decay, and Compton scattering.[1] On the other hand, the interaction of a virtual photon (γ_V) of large negative mass-squared (Q^2) with a nucleon is known to exhibit behavior not easily explained[2] by VMD, but rather, most easily understood in terms of pointlike constituents (partons or quarks), in particular, scaling and jet structure.[3] The connection between these two views lies in the low-Q^2 region, since at the lower end ($Q^2 \simeq 0$), VMD must be as valid as it is for real photons, while for $Q^2 \geq 1$ GeV^2, the simpler effects of individual partons are revealed.

A complete picture would unify these two seemingly disparate viewpoints, perhaps by regarding the fundamental interaction as that of the photon materializing into a quark-antiquark pair (analogous to e^+e^- pair production); the $q\bar{q}$ pair would exhibit the characteristics of a particular vector meson, depending on the probability that the $q\bar{q}$ wave function overlapped that of the vector meson.[4] Thus the whole question of confinement, as it relates to the $q\bar{q}$ wave function, would have to enter the final unification.

Within the $\gamma_V N$ interaction, the total cross section (measured by single-arm-spectrometer experiments[5]) and the exclusive production of vector mesons are most directly connected to VMD; the total cross section is related to the forward production of vector mesons by a generalized optical theorem[6] within VMD.

A significant difference between photoproduction and virtual-photon scattering, aside from the different Q^2, is the presence of a longitudinal (or scalar) component to the photon. The ratio of the total cross sections for longitudinal and transverse virtual photons on protons, $R = \sigma_L/\sigma_T$, is measured by single-arm-spectrometer experiments. The ratio of the cross sections for exclusive vector-meson production by longitudinal and transverse virtual photons, $R_V = \sigma_L(\gamma_V p \to Vp)/\sigma_T(\gamma_V p \to Vp)$, can be measured by observing the vector-meson decay angles, if s-channel helicity conservation (SCHC) is assumed. This assumption is associated with diffractive ρ production. The extra degree of freedom provided by longitudinal photons makes the physics of virtual-photon interactions a rich one, but, unfortunately, introduces largely unknown parameters into the theories, making definitive conclusions more difficult.

The exclusive production of vector mesons by photons,

$$\gamma_V p \to Vp,$$

has been treated theoretically from the VMD point of view[7,8] and by several other approaches.[9,10] Because these models do not provide a numerical value for R_V, their predictions in some cases are not strong, but some tests can be made, as will be seen later.

B. Kinematics and phenomenology

Leptoproduction of a vector meson is illustrated in Fig. 1, in which the various Lorentz four-vectors are defined. The invariants most commonly used in the analysis of this reaction are

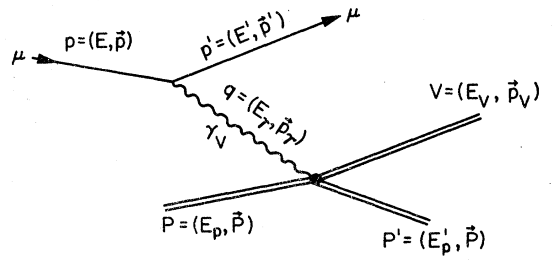

FIG. 1. The reaction $\mu p \to \mu p V$, assuming mediation via a single virtual photon.

the total hadronic center-of-mass energy $W = s^{1/2} = [(P+q)^2]^{1/2}$,

the negative mass-squared of the photon $Q^2 = -q^2$,

the momentum-transfer squared from the virtual photon to the vector meson $t = (V-q)^2$.

The laboratory energy of the virtual photon, $\nu = E - E'$, can be obtained from these invariants by $\nu = (s - M^2 + Q^2)/(2M)$, where M is the target-proton mass.

To compare virtual-photon cross sections with those of photoproduction, we require a convention for the flux of virtual photons in a leptoproduction experiment.[11] We take

$$\frac{d^2\sigma_{lp}}{dQ^2 dW} = \Gamma(\sigma_T + \epsilon\sigma_L),$$

where

$$\Gamma = \frac{\alpha}{4\pi^2}\,\frac{(W^2-M^2)}{MQ^2}\,\frac{(E-\nu)}{E(1-\epsilon)}$$

is the transverse-virtual-photon flux, and ϵ is the polarization discussed below. When we give the cross section σ_V for a particular vector meson to be produced via the reaction

$$\gamma_V \to Vp,$$

we mean the combination $\sigma_T + \epsilon\sigma_L$.

The transverse component of the virtual photon is polarized in the lepton scattering with a polarization given by

$$\epsilon = \frac{1}{1+a}, \quad a = \frac{2(\nu^2+Q^2)}{4E(E-\nu)-Q^2}.$$

Thus, as $E \to \infty$ with fixed ν and Q^2, we have $\epsilon \to 1$, i.e., 100% polarization. On the other hand, if ν remains a fixed fraction f of the initial energy, then $a \to \frac{1}{2}f^2/(1-f)$ as $E \to \infty$. The longitudinal photons are coherent with the polarized portion of the transverse photons, allowing the possibility of observing transverse-longitudinal interference effects.

To measure polarization effects, the following angles must be defined (using the ρ meson for definiteness):

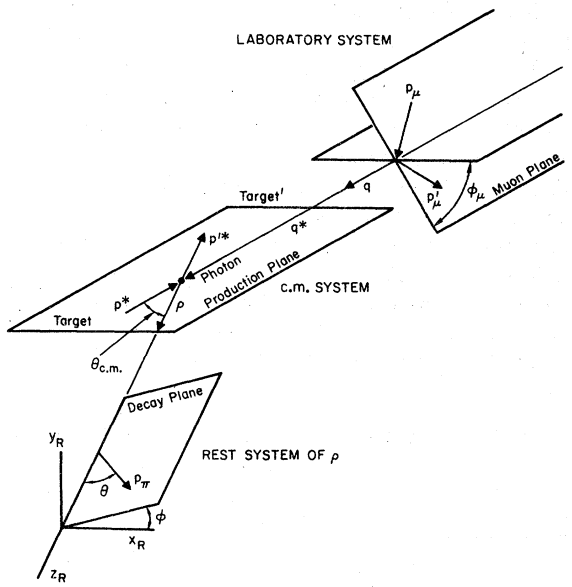

FIG. 2. Coordinate systems and angles used in the density matrix decomposition for ρ decay.

ϕ_l = the azimuthal angle between the lepton-scattering plane and the vector-meson production plane.

θ, ϕ = polar and azimuthal angles for the π^+ from ρ decay.

The angles θ, ϕ are defined in the ρ-meson rest frame. The z axis is taken to be the direction of the ρ in the hadronic center-of-mass system (helicity frame). See Fig. 2 for a description of these angles and coordinate systems. We follow Dakin *et al.*[12] in defining an angle $\psi \equiv \phi_l + \phi$.

The complete description of the vector-meson decay matrix elements in terms of these angles is given in the Appendix. It is useful here to point out that if SCHC is valid, the normalized angular distribution of ρ decay is given by

$$W(\theta,\psi) = \frac{3}{4\pi(1+\epsilon R_\rho)}\{\tfrac{1}{2}\sin^2\theta(1+\epsilon\cos 2\psi) + \epsilon R_\rho \cos^2\theta - [\epsilon R_\rho(1+\epsilon)/2]^{1/2} \times \cos\delta \sin 2\theta \cos\psi\}.$$

where δ is the phase angle between the amplitudes for longitudinal and transverse ρ production.

C. Exclusive photoproduction of vector mesons

The photoproduction of vector mesons at laboratory momenta of greater than 3 GeV/c has been shown to have a roughly energy-independent cross section and an exponential momentum-transfer dependence (with an energy-independent slope parameter $A \approx 7$ GeV^{-2}).[13,14] In addition, natural-parity

exchanges and amplitudes obeying SCHC have been shown to be dominant. All these observations identify the production process as diffractive.

A definite mass skewing has been observed in the case of the rather broad ρ; the skewing has been fitted by employing an additional factor multiplying the ρ Breit-Wigner form. The factor has been parametrized by $(M_\rho/M_{\pi\pi})^{n(t)}$, where $n(t)$ has been experimentally observed[13] to be a rapid function of t $[n(t)\approx 6(1+t/0.6\ \mathrm{GeV}^2)]$, which, when averaged over the exponential t distribution, yields $\langle n\rangle_t \approx 4$. No satisfactory theory has yet explained the remarkable t dependence of $n(t)$, despite several attempts.[14-16]

D. Previous results on vector-meson production by virtual photons

A number of other experiments have presented results on ρ production by virtual photons in the $0<Q^2<5$ GeV^2 range.[12,17-20] Preliminary versions of our data have also been presented.[21] These results have demonstrated that the cross section for ρ production decreases as a function of Q^2; whether that decrease agrees with the predictions of VMD has been a subject of controversy.

The Q^2 dependence of the t slope for ρ production is of interest because of the question of "photon shrinkage," expected perhaps as the photon more efficiently probes the pointlike constituents in the proton. Although a number of claims for a decrease in A as Q^2 increases have been made in the literature (see, for example, Ref. 12), the data are in fact consistent with no Q^2 dependence.[22]

The mass skewing of the ρ has been measured at Q^2 values below 1 GeV^2 and has been found to be identical to the photoproduction result within errors. Above $Q^2=1$ GeV^2, few results are available.

Analysis of the ρ decay angular distribution has revealed that SCHC amplitudes remain dominant out to Q^2 values above 1 GeV^2. The production of longitudinally polarized ρ's has been clearly observed. Since the production cross section for longitudinally polarized ρ's must go to zero at $Q^2=0$, the ratio R has been parametrized as $R_\rho=\xi^2Q^2/M_\rho^2$. [Within the VMD picture the quantity ξ is the ratio of the forward elastic ρp cross section for longitudinally and transversely polarized ρ's; i.e., $\xi=\sigma_L(\rho p\to\rho p)/\sigma_T(\rho p\to\rho p)$.] For $Q^2<1$ GeV^2, the data are consistent with ξ^2 between 0.3 and 0.7, but above $Q^2=1$ GeV^2 few results are available. The phase angle δ has been measured to be near zero in all experiments where $W>2.5$ GeV; that is, maximal longitudinal-transverse interference is observed, consistent with both processes being diffractive.

The leptoproduction of ω mesons contains substantial unnatural-parity exchange[23] for W values below about 2.5 GeV. Hence, for comparisons with VMD calculations, one should restrict oneself to relatively high energy. Only Ref. 23 and our experiment have relatively high-energy data; these data are discussed in Sec. IV.

Most of the leptoproduction experiments that observe final states have at most a few ϕ mesons, due to the low cross section for ϕ leptoproduction. However, Dixon *et al.*[24] have observed a substantial number of ϕ mesons up to $Q^2\simeq 1$ GeV^2. They observe no photon shrinkage, find SCHC and $R_\phi \simeq R_{\rho'}$, and find a Q^2 dependence to the ϕ production cross section consistent with VMD.

E. Summary of results from this experiment

We have performed a muon-proton scattering experiment at the Stanford Linear Accelerator Center (SLAC) to study the final-state hadrons produced at 14-GeV/c incident laboratory muon momentum. In this paper, we present our final results for the reactions

$$\mu p\to\mu p\rho^0\to\pi^+\pi^-,$$

$$\mu p\to\mu p\omega\to\pi^+\pi^-\pi^0,$$

$$\mu p\to\mu p\phi\to K^+K^-.$$

Our results cover the kinematic range $1.7<W<4.7$ GeV and $0.3<Q^2<5$ GeV^2. Table I lists the quantities we have measured for these three reactions.

Our results provide further evidence for the picture of vector-meson production presented in Sec. I D. Additional conclusions which have come primarily from this experiment, or which can be reached only after consideration of several experiments, including ours, are the following:

(1) The ratio of ω to ρ^0 production remains constant at the photoproduction value out to $Q^2>2$ GeV^2, as expected if naive VMD is valid.

(2) In ρ^0 production, both the skewing parameter $\langle n\rangle_t$ and the parameter ξ^2 in the expression for the longitudinal-transverse ratio show a significant decrease above $Q^2=1$ GeV^2.

(3) The cross section for ρ^0 production as a function of Q^2 falls below the VMD prediction, when the measured ξ^2 parameter is taken into account.

II. EXPERIMENTAL METHOD

A. Description of apparatus

A complete description of the apparatus can be found in Refs. 25, 26, and 27. Here we provide a brief summary, pointing out the principal features of interest. The apparatus is shown in Fig. 3. The experiment utilized a 14-GeV positive muon beam of intensity 180 muons per SLAC pulse. The beam

TABLE I. Quantities measured in this experiment. The W and Q^2 regions are in some cases divided further into bins.

Meson	Quantity	W region (GeV)	Q^2 region (GeV^2)	$\|t\|$ region (GeV^2)
ρ^0	$\sigma_\rho\,(Q^2)$	1.7–4.7	0.3–5	
	$\langle n\rangle_t$	2–4.7	0.3–5	<0.6
	A	2–4.7	0.3–5	<0.6
	Density matrix	2.5–4.7	0.3–5	<0.6
	R_ρ	2.5–4.7	0.3–5	<0.6
	$\cos\delta$	2.5–4.7	0.3–5	<0.6
ω	$\frac{\sigma_\omega\,(Q^2)}{\sigma_\rho\,(Q^2)}$	2.0–4.7	0.3–5	$\gtrsim 0.2$
	Upper limit to σ_ϕ	2.0–4.7	0.3–5	

was incident on a 40-cm-long liquid-hydrogen target contained within a $2\times0.8\times0.6$ m^3 streamer chamber. The beam traversed the streamer chamber in a 5-cm-diameter tube, made of Lexan. The chamber was immersed in a 16-kG magnetic field. The target was surrounded by a 9-cm-wide rectangular box, made of thin Mylar walls. The box was open to the air and provided a dead region around the target. This dead region was necessary due to the intense rate of δ-ray production caused by the fact that the beam pulse was much shorter than the streamer-chamber memory time. A trigger hodoscope consisting of four banks of scintillation counters, interspersed with 1.5 m of lead hadron absorber, was located directly behind the chamber. A trigger occurred if a muon penetrated all four scintillation planes in the hodoscope. All counters in the hodoscope were latched. This information was used for event reconstruction to aid in the identification of the muon.

B. Scanning and measuring

A total of 237 000 event candidates were photographed. All pictures were scanned twice, and disagreements were resolved by a third (conflict) scan. An event was recorded in the scan if it had one positive track consistent with being a triggering muon, accompanied by at least one other positive track. The efficiency for a single scan was measured to be 98%. All 44 000 event candidates were measured on conventional film-plane digitizers. The setting error for the measurement was 300 μ in space (demagnification 67). The events which failed reconstruction were measured a second and, if necessary, a third time.

C. Track and vertex reconstructions

Event reconstruction was accomplished via a set of programs known as SIOUX, consisting of (1) TVGP,[28] which determined track parameters in real space (2) APACHE,[29] which reconstructed the vertex by extrapolating tracks back into the target, and (3) SQUAW,[30] which attempted to fit the reconstructed vertex with specific kinematical hypotheses. An event candidate survived the reconstruction procedure if APACHE could successfully find a vertex consisting of a muon and at least one positive hadron. The muon in each event was identified by finding a track which could be extrapolated through the trigger hodoscope in a manner consistent with the counter latch information. The remainder of the tracks included in the vertex by APACHE were assumed to be due to hadrons.

The number of positive final-state hadrons in the reaction $\mu p \to \mu +$ hadrons should exceed the number of negative hadrons by one. However, due to hadronic track losses, some of the vertices reconstructed by APACHE did not meet this condition. We refer to such vertices as "charge-unbalanced." The overall efficiency for detecting charged hadrons was determined to be about 86%. The factors contributing to the losses were (1)

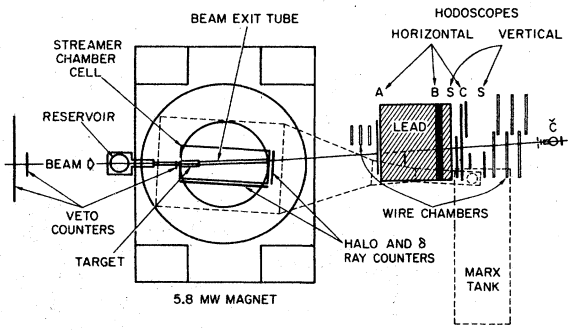

FIG. 3. Plan view of the detection apparatus. The hodoscope and lead wall had openings for the unscattered beam and the streamer-chamber pulsing system.

tracks which failed to emerge from the target box (9%), (2) scattered tracks which could not be extrapolated back to the vertex (2%), (3) tracks obscured by the beam exit tube (2%), and (4) errors made in measuring (0.5%).

The final event sample consisted of 10 463 events of which 7620 were inelastic events with $Q^2 > 0.3$ GeV^2.

D. Selection of particular final states

Squaw attempted four-constraint (4C) fits to the hypotheses

$$\mu p \to \mu p \pi^+ \pi^-, \quad \text{(A)}$$

$$\mu p \to \mu p K^+ K^- \quad \text{(B)}$$

and one-constraint (1C) fits to the reaction

$$\mu p \to \mu p \pi^+ \pi^- \pi^0. \quad \text{(C)}$$

These fits were attempted for all events containing one negative and two positive hadrons.

We investigated the reconstruction program's ability to exclude extraneous tracks from the vertex (mainly beam halo and δ rays) by attempting to obtain 4C fits to subsets of hadrons emanating from higher-multiplicity vertices. The results of this study indicated that less than 1% of the 4C fits to reactions (A) and (B) above came from a subset of tracks identified by APACHE as constituting a vertex. These events were therefore considered to be genuine higher-multiplicity events, and not candidates for the reactions under study.

One-constraint fits to reactions (A) and (B) were attempted for all charge-unbalanced event vertices having exactly two charged hadrons.

1. $\mu^+ p \pi^+ \pi^-$

This final state appears in both 4C and 1C fits; to extract t distributions and decay-angle distributions without large biases, the 1C fit must be included in the sample. However, the 1C fits suffer from substantial background contamination and also from the twofold ambiguity in determining which positive hadron is the proton. A few of the 4C fits also have the twofold proton ambiguity. A special scan was performed to resolve these difficulties. All events containing 1C fits or ambiguous 4C fits to reaction (A) were examined in a special scan by a physicist for consistency with event topology and, where possible, for ionization appropriate to the assumed masses of the particles. A 1C fit was retained if (1) there was evidence for a track consistent with the fit hypothesis that, for some reason, did not survive vertex reconstruction (scattered tracks, measuring errors, etc.), or (2) the fit hypothesis predicted a track with parameters that gave it a small probability

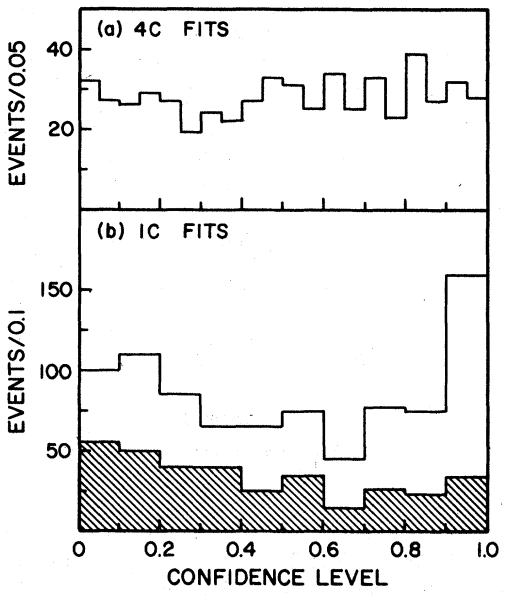

FIG. 4. Confidence-level distributions for fits to the reaction $\mu p \to \mu p \pi^+ \pi^-$. (a) 4C fits with $\chi^2 < 12.5$, (b) 1C fits with $\chi^2 < 7$. The shaded region shows those events that passed the special 1C fit scan.

for being observed (insufficient momentum to leave target, etc.). Approximately $\frac{2}{3}$ of the 1C fits were rejected. The rejected 1C fits were mostly events that contain neutrals in addition to the missing charged track. The fit hypotheses in these cases predict a charged hadron with kinematical parameters that account for all the unobserved momentum in the event. Since the charged hadron detection efficiency was high, the validity of these fits could usually be determined, with a high degree of certainty, by scanning the event for evidence of the predicted track in the streamer chamber.

A sample of events fitting both reaction (A) and reaction (B) was also included in this scan. From a study of the ionization in these events, we concluded that contamination from the latter reaction is negligible.

The final event sample consisted of 566 events with a 4C fit ($\chi^2 < 12.5$) and 338 events with a 1C fit ($\chi^2 < 7$) that survived the special scan. The probability distributions for these two classes of fits are shown in Fig. 4.

2. $\mu^+ p K^+ K^-$

Many of the events that fit this final state may in fact be events of reaction (A), but if we concentrate on the ϕ-meson contribution, the narrowness of the ϕ allows an elimination of almost all background. The experimental resolution for the K^+K^- invariant mass in the ϕ-meson region is about

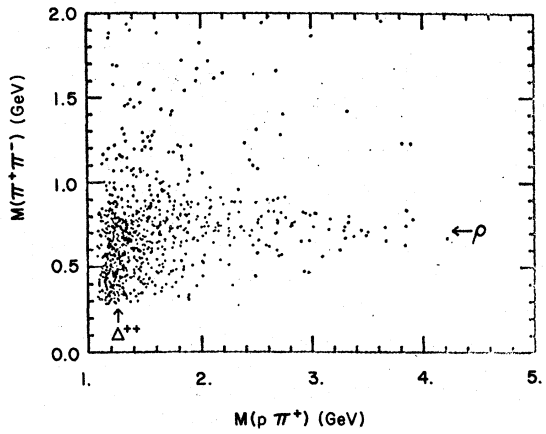

FIG. 5. A scatter plot of $M_{\pi\pi}$ vs $M_{p\pi^+}$ for the reaction $\mu p \to \mu p \pi^+ \pi^-$.

10 MeV [full width at half maximum (FWHM)]. A total of 24 events fit this final state with K^+K^- mass less than 1450 MeV

3. $\mu^+ p \pi^+ \pi^- \pi^0$

This final state requires a 1C fit. As in the $\mu^+ p K^+ K^-$ final state, contamination from erroneous fits may be large. However, if we concentrate on the ω-meson contribution, the narrowness of the ω will allow an elimination (or estimation) of almost all background. The experimental resolution for the $\pi^+\pi^-\pi^0$ invariant mass in the region of the ω meson is about 35 MeV (FWHM). A total of 451 events fit this final state with $W > 2$ GeV.

III. EXCLUSIVE ρ^0 PRODUCTION BY VIRTUAL PHOTONS: THE REACTION $\gamma_V p \to \rho^0 p$

A. Introduction

Exclusive ρ^0 production appears in reaction (A), along with significant contributions from Δ^{++} and Δ^0 production. A scatter plot for this event sample is shown in Fig. 5. Both ρ and Δ^{++} signals are clearly present. To extract the ρ^0 contribution and to measure ρ^0 production and decay properties, maximum-likelihood fits were performed, using OPTIME.[31] A matrix element was constructed to account for ρ^0 production and three "background" reactions: Δ^{++}, Δ^0 production, and phase space. The square of the invariant matrix element was taken to be

$$|M|^2 = a_1 F_{\rm BW}(M_{p\pi^+}) e^{Bt_{\pi^-}} + a_2 F_{\rm BW}(M_{p\pi^-}) e^{Bt_{\pi^+}} + a_3 F_{\rm BW}(M_{\pi\pi}) F_{\rm skew}{}^n e^{At'} W(\cos\theta) + a_4. \quad (1)$$

In this expression, $M_{p\pi^+}$, $M_{p\pi^-}$, and $M_{\pi\pi}$ represent the invariant masses of the two-body combinations $p\pi^+$, $p\pi^-$, and $\pi^+\pi^-$, respectively; t_{π^-} and t_{π^+} are the squares of the four-momentum transfers from the virtual photon to the π^- and π^+, respectively, and θ is the lab angle between the pions. The factor $F_{\rm skew}$ is inserted to account for the skewed ρ^0 mass shape mentioned in Sec. IC. It is discussed in detail in Sec. III B on the mass spectra. The quantity t' is defined as

$$t' = t - t_{\rm min},$$

where the minimum momentum transfer consistent with energy-momentum conservation $t_{\rm min}$ is given by

$$t_{\rm min} = (E_\gamma - E_\rho)^2 - (P_\gamma - P_\rho)^2 \cong -\frac{M^2(M_\rho{}^2 + Q^2)^2}{s^2}.$$

Here E_γ and P_γ are the energy and momentum of the virtual photon, E_ρ and P_ρ, those of the dipion system, and M is the proton mass. In a few of the fits we have used t, rather than t'. In expression (1) $F_{\rm BW}$ represents a relativistic Breit-Wigner resonance term. The forms of the resonances

TABLE II. Percentage channel contributions to the reactions $\mu^+ p \to \mu^+ p \pi^+ \pi^-$, determined from maximum-likelihood fits.

W (GeV)	$\overline{W}$	Q^2 (GeV^2)	$\overline{Q}^2$	Number of events	$p\rho^\circ$	$\Delta^{++}\pi^-$	$\Delta^\circ\pi^+$	Phase space
1.7–2.0	1.85	0.3–0.6	0.48	77	43 ± 9	29 ± 11	•••	28 ± 9
	1.83	0.6–1.0	0.76	86	33 ± 8	18 ± 10	4 ± 8	45 ± 13
	1.85	1.0–5.0	1.40	57	22 ± 8	24 ± 11	24 ± 10	30 ± 15
2.0–2.5	2.19	0.3–0.6	0.49	60	47 ± 10	4 ± 5	•••	49 ± 12
	2.18	0.6–1.0	0.77	84	34 ± 9	17 ± 7	•••	49 ± 9
	2.21	1.0–5.0	1.60	77	41 ± 8	0 ± 9	•••	59 ± 11
2.5–4.7	3.22	0.3–0.6	0.46	50	82 ± 13	•••	•••	18 ± 7
	3.10	0.6–1.0	0.80	70	61 ± 10	•••	•••	39 ± 8
	3.03	1.0–5.0	1.45	67	73 ± 11	•••	•••	27 ± 7

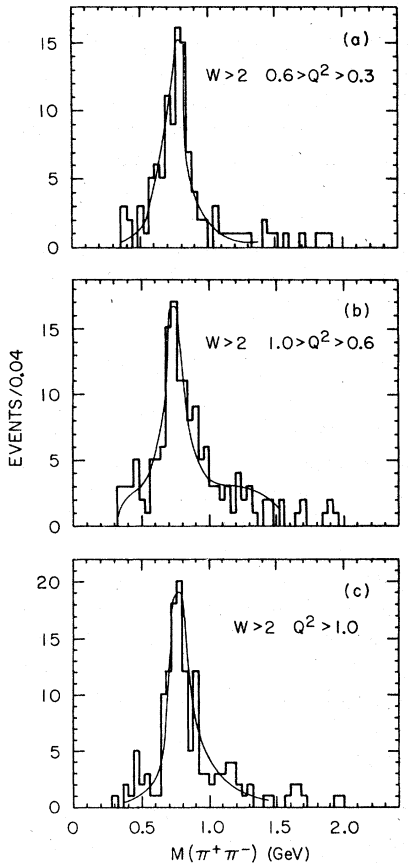

FIG. 6. Histograms of $M_{\pi\pi}$ for events of the reaction $\mu p \to \mu p \pi^+ \pi^-$ with $W > 2$ GeV. The curves are explained in the text.

were the same as those used in photoproduction[13] and include an energy-dependent width. The function $W(\cos\theta)$, the angular distribution of ρ^0 decay, is defined in the Appendix.

The quantities a_1 through a_4 measure the fractional contributions for the Δ^{++}, Δ^0, ρ^0, and phase-space background, respectively. Table II lists the results for the fractional contributions of each channel obtained from fits to a number of different W and Q^2 bins. The ρ^0 parameters that went into these fits will be discussed in detail in the following sections. The only unknown Δ parameter is the t slope B. Photoproduction experiments indicate that the t dependence of Δ production for $0.2 < t < 1$ GeV^2 can be parametrized by a factor of e^{Bt}, with B between 3 and 5 GeV^{-2}, depending on energy. We have fixed B in most of our fits at 4 GeV^{-2}. In a few cases, we reran the fitting program with B variable or with B fixed at 3 or 5 GeV^{-2}. Our ρ^0 results are insensitive to such changes in the fitting procedure.

B. Mass spectra

The mass spectra for the $p\pi^+\pi^-$ hadronic final state are shown in Figs. 6 and 7 for $W > 2$ GeV. Clear ρ^0 and Δ^{++} signals are seen, and a small Δ^0 signal is observed. A marked skewing of the ρ is observed in photoproduction. In our data we see clear evidence for skewing at low Q^2 [Fig. 6(a)], a result compatible with other virtual-photon experiments.[12,18-20] At $Q^2 > 1$ GeV^2 we see an *absence* of skewing [Fig. 6(c)], a result previously only suggested by Ref. 12. If we attempt to parametrize the ρ^0 shape with $F_{\text{skew}} = M_\rho / M_{\pi\pi}$ and the exponent n either a constant ($n = 4$) or $n(t) = 6(1 - |t|/0.6$ GeV^2), we find that the high-Q^2 distribution is very poorly fitted. Thus some Q^2 dependence of the skewing is required by our data. We have tried fits with two different types of Q^2-dependent F_{skew} factors:

$$F^{\text{II}}_{\text{skew}} = [(M_\rho^2 + Q^2)/(M_{\pi\pi}^2 + Q^2)]^{1/2},$$
$$F^{\text{III}}_{\text{skew}} = [(M_\rho^2 + Q^2 + |t|)/(M_{\pi\pi}^2 + Q^2 + |t|)]^{1/2}.$$

The factor $F^{\text{II}}_{\text{skew}}$ was suggested by Ross and Stodolsky[15] and the factor $F^{\text{III}}_{\text{skew}}$ was proposed by Kramer and Quinn.[9] Unfortunately, neither of these models has an explanation for the sharp t dependence observed in photoproduction. We have found no significant difference in the fits to our data using $F^{\text{II}}_{\text{skew}}$ or $F^{\text{III}}_{\text{skew}}$; both fit adequately with a constant exponent $n = 4$ or with a t-dependent exponent. We have also separately fitted in t bins for all events ($0.3 < Q^2 < 4.7$ GeV^2) and have found results consistent with our overall fits; the low-t bin ($0 < |t| < 0.25$ GeV^2) requires skewing whereas the high-t bin does not.

To summarize we show the fitted exponent n as a function of Q^2 from fits with $F_{\text{skew}} = M_\rho / M_{\pi\pi}$. Since we have taken n as independent of t we may regard the result as $\langle n \rangle_t$:

Q^2 (GeV^2)	$\langle n \rangle_t$
0.3–0.6	4.7 ± 0.8
0.6–1.0	5.0 ± 0.8
1.0–4.5	0.0 ± 1.3

Figure 8 shows our results along with similar fits from other experiments. Our high-Q^2 result, along with that of Dakin *et al.*,[2] establishes a significant change in $\langle n \rangle_t$ for $Q^2 > 1$ GeV^2.

Cross sections and other ρ properties have all been obtained with fits using $F^{\text{III}}_{\text{skew}}$ and $n = 4$. No significant difference in cross sections or other properties was found for fits using other satisfactory skewing parametrizations.

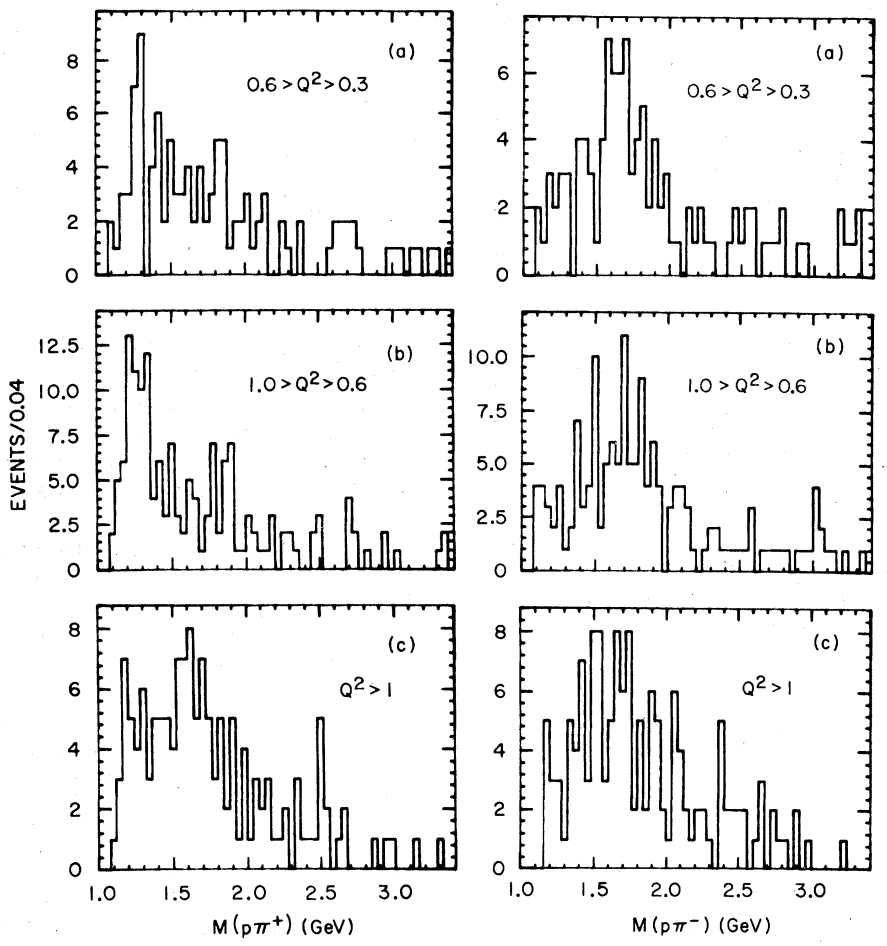

FIG. 7. Histograms of $M_{p\pi^+}$ and $M_{p\pi^-}$ for the reaction $\mu p \to \mu p \pi^+ \pi^-$ with $W > 2$ GeV.

C. Momentum-transfer distributions

The t dependence of exclusive ρ^0 production is parametrized by the factor e^{At}. It has been suggested that the coefficient A may fall with Q^2, due to shrinkage of the hadronic "size" of the virtual photon.

We investigated the slope A as a function of Q^2. To ensure that a diffractive mechanism dominates, the data were restricted to $2.2 < W < 4.7$ GeV and $t \leq 0.6$ GeV^2. They were then divided into three Q^2 bins in such a way that these bins have approximately equal statistical weight. Fits were performed using both t and $t' = (t - t_{\min})$; the results for the slope are presented below:

Exponential t slope A (GeV^{-2})

Q^2 (GeV^2)	t fit	t' fit
0.3–0.6	6.2 ± 1.0	6.1 ± 1.0
0.6–1.0	6.2 ± 1.2	6.6 ± 1.2
1.0–4.5	4.9 ± 1.0	5.8 ± 1.1

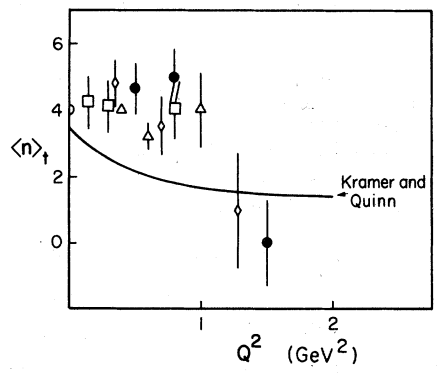

FIG. 8. Skewing exponent for the ρ mass shape as a function of Q^2. The curve is based (Ref. 18) on the theory of Kramer and Quinn (Ref. 9), who predict the SK_{III} skewing factor with $n = 4$. The experimental points come from ● this experiment; △ Joos *et al.*, Ref. 19; □ Ballam *et al.*, Ref. 18; ◇ Dakin *et al.*, Ref. 12; ○ Ballam *et al.*, Ref. 13.

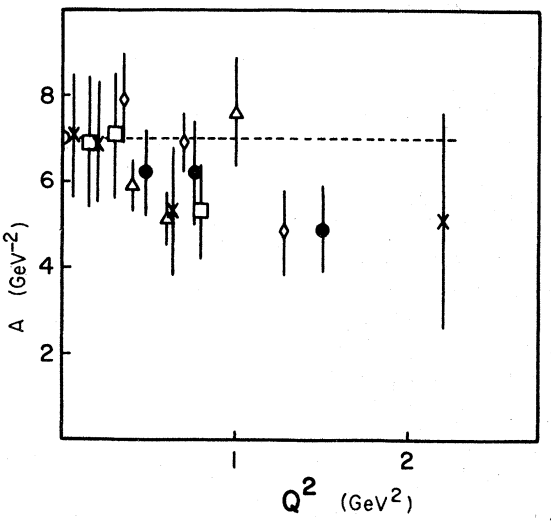

FIG. 9. Experimental t slope for ρ production as a function of Q^2. The experimental points come from ● this experiment; △ Joos *et al.*, Ref. 19; □ Ballam *et al.*, Ref. 18; ◇ Dakin *et al.*, Ref. 12; × Francis *et al.*, Ref. 20; ○ Ballam *et al.*, Ref. 13.

Figure 9 shows our results for A as a function of Q^2, along with those of other experiments. We see no significant change with Q^2 in the A slope, although the data are consistent with a slight decrease with Q^2. Fractional cross sections given in Table II were determined from fits with A fixed at 6 GeV^2.

D. ρ^0-Decay angular distributions

The density matrix elements for ρ production can be obtained from an analysis of the angular distribution of the pions resulting from the ρ decay. The coordinate system and angles have been defined in Sec. I B, and the density matrix elements are defined in the Appendix.

TABLE III. Density matrix elements for exclusive ρ production. Selections are $W > 2.5$ GeV, $Q^2 > 0.6$ GeV^2, $0.6 < M_{\pi\pi} < 0.9$ GeV, $|t| < 0.6$ GeV^2. Average values are $\overline{W} = 3.14$ GeV, $\overline{Q}^2 = 0.90$ GeV^2, $|\overline{t}| = 0.87$ GeV^2. There are 93 events in the sample. Elements with an asterisk should be zero if SCHC is valid.

r^4_{00}	0.45 ± 0.08	$\mathrm{Im}\, r^2_{10}$*	-0.07 ± 0.09
$\mathrm{Re}\, r^4_{01}$*	0.05 ± 0.05	$\mathrm{Im}\, r^2_{1-1}$	-0.33 ± 0.12
r^{04}_{1-1}*	0.10 ± 0.07	r^5_{00}*	0.09 ± 0.07
r^1_{00}*	0.12 ± 0.15	r^5_{10}	0.14 ± 0.03
$\mathrm{Re}\, r^1_{10}$*	-0.03 ± 0.07	r^5_{11}*	-0.02 ± 0.04
r^1_{11}*	0.05 ± 0.07	r^5_{1-1}*	-0.03 ± 0.06
r^1_{1-1}	0.10 ± 0.12	r^6_{10}	-0.09 ± 0.04
		r^6_{1-1}*	0.00 ± 0.06

TABLE IV. Values for R_ρ and δ for different Q^2 bins. The W selection is $W > 2.5$ GeV.

Q^2 (GeV^2)	R	$\cos\delta$
0.3–0.6	0.63 ± 0.35	0.24 ± 0.26
0.6–1.0	2.4 ± 1.4	0.79 ± 0.20
1.0–5.0	0.52 ± 0.29	0.88 ± 0.13

The density matrix elements have been determined for events lying in the ρ resonance region using the method of moments. (It should be noted that this method does not properly treat background events lying underneath the ρ.) The results obtained for the matrix elements are shown in Table III.

For the case of s-channel helicity conservation (SCHC), matrix elements composed of helicity-flip amplitudes should be 0. These are indicated by an asterisk in Table III. The results are reasonably consistent with SCHC; however, small violations cannot be ruled out. We note that in ρ photoproduction, where there are sufficient data to study the helicity-flip terms in detail, there is evidence for small violations of s-channel helicity conservation.[13,14]

If SCHC is correct, and if ρ^0 production proceeds via natural-parity exchange in the t channel, then the angular distribution for ρ decay can be written in terms of R_ρ and the phase angle δ. The expression for the normalized angular distribution is given in Sec. I B.

We have performed maximum-likelihood fits utilizing this decay distribution. The results for R and $\cos\delta$ as a function of Q^2 are shown in Table

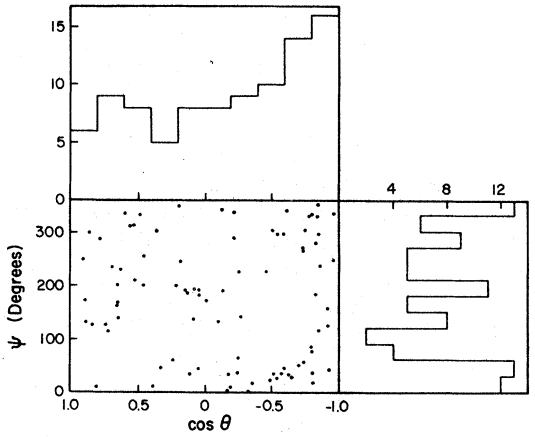

FIG. 10. Scatter plot of $\cos\theta$ vs ψ for ρ decay. Selections are $0.6 < M_{\pi\pi} < 0.9$ GeV, $Q^2 < 0.6$ GeV^2, and $W > 2.5$ GeV.

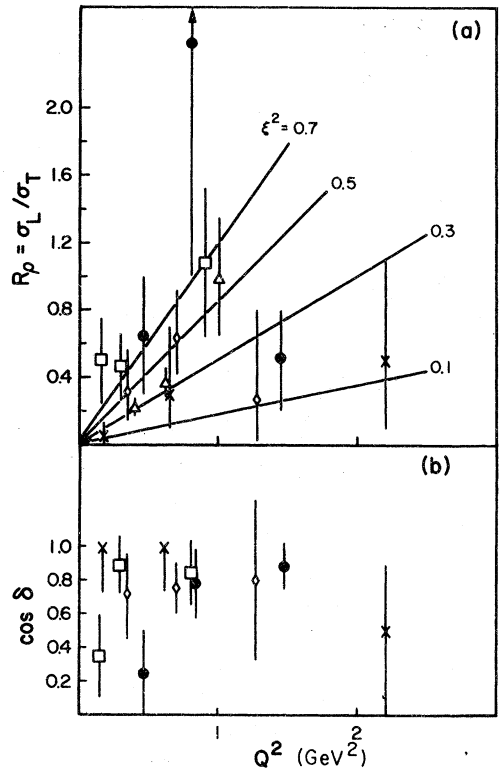

FIG. 11. Longitudinal-transverse interference parameters for ρ production, determined from ρ decay angular distributions. Our results are from maximum-likelihood fits to events with $W > 2.5$ GeV. The experiments are indicated by the same symbols as those used in Fig. 9. (a) Longitudinal-transverse ratio, R_ρ, (b) phase angle, δ.

IV. The fact that the amplitudes are nearly in phase can be observed in the scatter plot of Fig. 10, which shows the effect of the interference term in the expression for $W(\cos\theta, \psi)$.

Figure 11 shows our results for R_ρ and δ along with the results of other experiments. We see a very clear indication that the parameter ξ is not constant, but decreases significantly at Q^2 of order 1 GeV^2. In the VMD model this would imply a decrease in $\sigma_L(\rho p \to \rho p)$ relative to $\sigma_T(\rho p \to \rho p)$.

E. Q^2 dependence of the ρ^0 cross section

In the previous four sections, all the parameters necessary to define the full matrix element for exclusive ρ^0 production were discussed in detail, and the procedure for obtaining the fractional ρ cross sections in Table II have thus been explained. We now extract the absolute cross section for the reaction $\mu^+ p \to \mu^+ p \rho^0$. We define

$$\sigma_\rho = (\sigma_\rho/\sigma_{\pi\pi})(\sigma_{\pi\pi}/\sigma_{\rm tot})\langle \sigma_T + \epsilon\sigma_L \rangle .$$

The fractional cross section $\sigma_\rho/\sigma_{\pi\pi}$ is obtained from Table II. To obtain $\sigma_{\pi\pi}/\sigma_{\rm tot}$, we must consider events of all topologies within the particular W and Q^2 bins of interest. We assign a weight w equal to the inverse of the muon detection efficiency for each event, at its particular W, Q^2 value. We assign an additional weight h to the one-prong events. The ratio of $\sigma_{\pi\pi}$ to the total inelastic cross section $\sigma_{\rm tot}$ is then defined as

$$\frac{\sigma_{\pi\pi}}{\sigma_{\rm tot}} = \frac{\sum' w_i}{\sum w_i + \sum w_i h_i}$$

where $\sum'$ is a sum over all $\mu p \pi\pi$ events and $\sum$ is a sum over all events. The w's account for possible differences in the way the vector-meson events and the total inelastic data sample populate the Q^2-W bins. The weight h corrects the inelastic sample for lost one-prong events, since these do not survive the analysis procedure if the hadron goes unobserved. The average value of the weight h is

TABLE V. Absolute cross sections for exclusive ρ production. The absolute total cross section $\sigma_T + \epsilon\sigma_L$ was obtained from Ref. 32.

W (GeV)	Q^2 (GeV^2)	$\sigma_\rho/\sigma_{\rm tot}$	$\sigma_T + \epsilon\sigma_L$ (μb)	σ_ρ (μb)
1.7–2.0	0.3–0.6	0.082 ± 0.017	101.8	8.4 ± 1.7
	0.6–1.0	0.077 ± 0.018	73.7	5.6 ± 1.3
	1.0–5.0	0.041 ± 0.016	21.28	0.87 ± 0.33
2.0–2.5	0.3–0.6	0.064 ± 0.014	81.8	5.2 ± 1.1
	0.6–1.0	0.056 ± 0.014	59.9	3.3 ± 0.8
	1.0–5.0	0.059 ± 0.012	20.79	1.23 ± 0.25
2.5–4.7	0.3–0.6	0.055 ± 0.009	63.8	3.49 ± 0.55
	0.6–1.0	0.052 ± 0.008	45.85	2.37 ± 0.38
	1.0–5.0	0.033 ± 0.005	19.28	0.64 ± 0.10
2.0–4.7	0.3–0.6	0.061 ± 0.008	67.3	4.08 ± 0.55
	0.6–1.0	0.055 ± 0.007	48.61	2.65 ± 0.34
	1.0–5.0	0.045 ± 0.005	19.61	0.88 ± 0.10

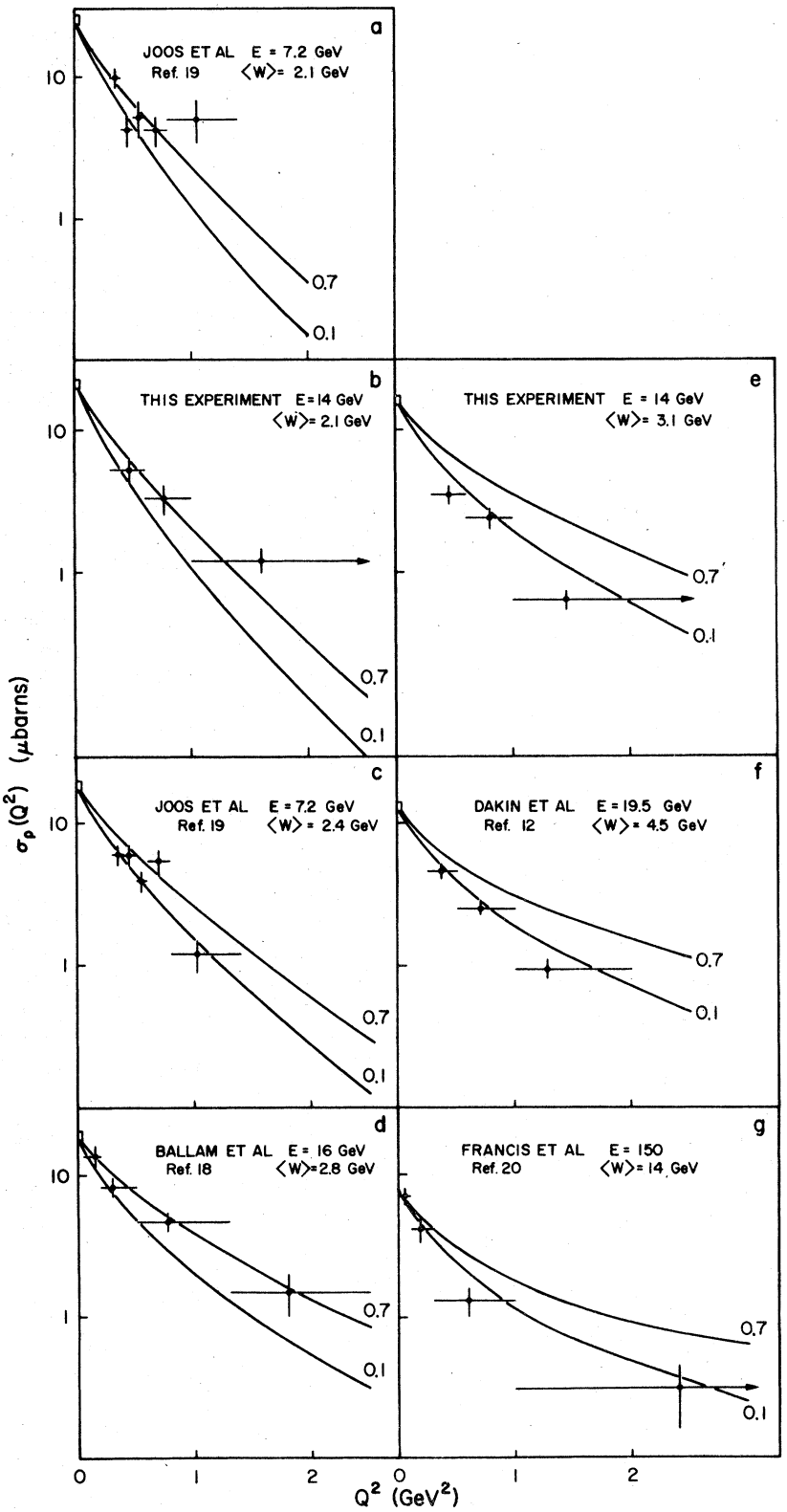

FIG. 12. Cross sections for ρ production as a function of Q^2 for a number of experiments at different W values and at different incident lepton energies E. The curves are the predictions of the VMD model (see text) for different values of ξ^2, a parameter whose independent measurements are shown in Fig. 11(a). The open squares at $Q^2=0$ are photoproduction points from Refs. 13, 14, and 20.

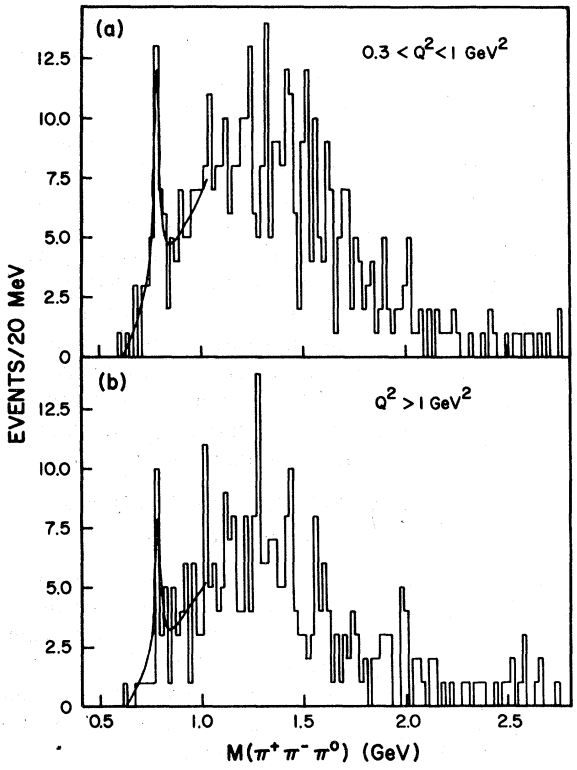

FIG. 13. Histograms of $\pi^+\pi^-\pi^0$ mass for events that fit the reaction $\mu p \to \mu p \pi^+\pi^-\pi^0$ with $W>2$ GeV. The curves are fits over the range $0.63<M_{3\pi}<1.03$ GeV to a linear background plus an ω resonance at known mass and of Breit-Wigner form with $\Gamma=35$ MeV (this simulates the calculated resolution function).

1.15.

The combination of $\sigma_T+\epsilon\sigma_L$ is a function of Q^2 and W. We have obtained $\sigma_T+\epsilon\sigma_L$ from a multiparameter fit to the single-arm spectrometer data.[32] The angular brackets enclosing $\sigma_T+\epsilon\sigma_L$ refer to an average over the Q^2 and W bin in question.

The resulting absolute cross sections for exclusive ρ^0 production are given in Table V. These cross sections, along with those of other experiments, are plotted as a function of Q^2 in Fig. 12.

TABLE VI. Comparison of ω production to four-constraint-fit ρ production. This comparison gives the ratio of ρ to ω production in the kinematic regions determined by track losses in the streamer chamber. The most important losses occur at $|t| \lesssim 0.2$ GeV^2. The selection is $W>2$ GeV.

Q^2 (GeV^2)	4C ρ events	ω events	$\sigma_\rho/\sigma_\omega$
0.3–1.0	105±12	23±5	4.6±1.1
1.0–5.0	75±9	15±4	5.0±1.5

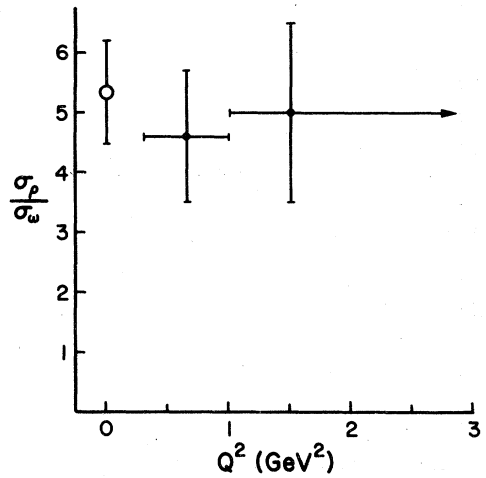

FIG. 14. The cross-section ratio of $\sigma_\rho/\sigma_\omega$ as a function of Q^2. The photoproduction value is from an experiment with the corresponding W value (~3.1 GeV) given in Ref. 13.

On each plot are shown curves predicted by the VMD model,[22] in a version that treats ξ as an unknown parameter. The predicted curves are given by

$$\sigma_\rho(Q^2)=\sigma_\rho(0)K\exp\{A[t_{\min}(Q^2)-t_{\min}(0)]\}\times\frac{(1+\epsilon\xi^2Q^2/M_\rho^2)}{(1+Q^2/M_\rho^2)^2},$$

where

$$K=(W^2-M_\rho^2)/[(W^2-M_\rho^2-Q^2)^2+4W^2Q^2]^{1/2}.$$

The K factor is always very close to unity for reasonable W and Q^2, as is the exponential factor. We have taken $\sigma_\rho(0)$, the ρ^0 photoproduction cross section, from experimental data.[13,14,20] The ρ propagator yields a significant decrease with Q^2, but that decrease is considerably modified by the factor involving ξ^2. Figure 11 shows that ξ^2 is significantly greater than 0.1; near $Q^2=1$ GeV^2 it is probably near 0.5. In view of this information,

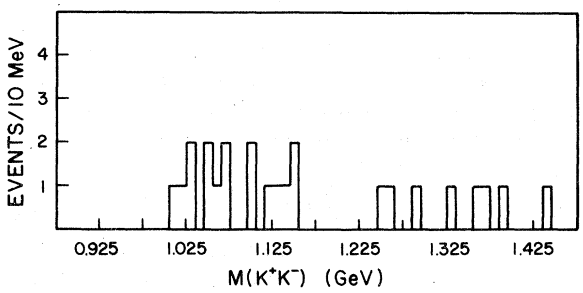

FIG. 15. Histogram of K^+K^- mass for events that fit the reaction $\mu p \to \mu p K^+K^-$ with $W>2$ GeV. The experimental resolution in the ϕ-meson region is calculated to be 10 MeV (FWHM).

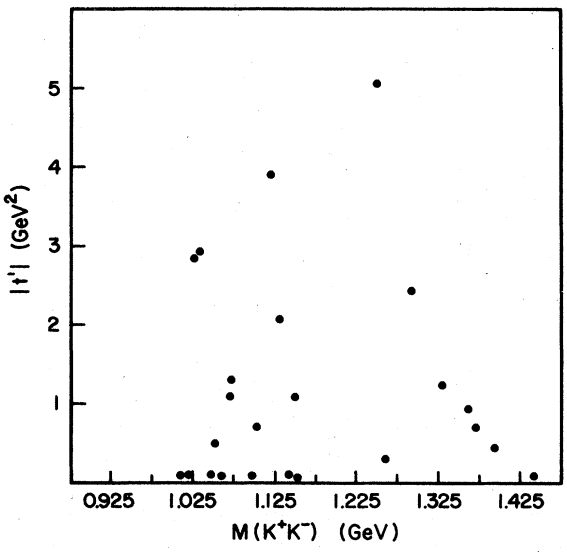

FIG. 16. Chew-low plot for K^+K^- events (the same events that appear in Fig. 15).

the data in Fig. 12 indicate that the observed cross sections are significantly lower than the VMD prediction.

IV. EXCLUSIVE ω PRODUCTION BY VIRTUAL PHOTONS: THE REACTION $\gamma_V p \to \omega p$

Exclusive ω production appears in reaction (C). As mentioned in Sec. I D, unnatural-parity-exchange contributions substantially affect low-energy ω production: We therefore restrict the events to $W > 2$ GeV. The three-pion mass distributions for all events that fit reaction (C) are shown in Fig. 13. The curves are from fits over the mass range 600–1010 MeV with a resonance at the known ω mass. The resolution at the ω mass was calculated for each event by SQUAW, and the resolution function formed from these calculations was found to fit a Breit-Wigner function with $\Gamma = 35$ MeV. This function was used in the fits, which also assumed a linear background. (It was found that use of a quadratic background did not change the number of ω mesons more than one standard deviation.)

The sample of ω mesons found in this manner is incomplete due to losses of slow protons in the streamer-chamber target box and other track losses. We cannot recover these events in a manner similar to the recovery of the analogous ρ-meson events, owing to the lack of constraints resulting from the missing π^0. However, we can calculate the ratio of ω to ρ production *within the particular kinematic region imposed by the track losses* by comparing the ω signal to the ρ signal obtained from 4C events only. Table VI and Fig. 14 show this comparison and the resulting $\sigma_\rho/\sigma_\omega$ as a function of Q^2. We see the striking result that the ρ/ω ratio remains essentially constant out to Q^2 above 1 GeV^2. This seems to imply that the fraction of the hadronic part of the photon that couples to vector mesons, while decreasing in strength with Q^2, retains its SU_3 coupling ratios. The data of Joos *et al.*[19,23] are apparently in contradiction with this result, indicating instead approximate equality of σ_ρ and σ_ω near $Q^2 = 1$ GeV^2.

V. UPPER LIMITS TO EXCLUSIVE ϕ PRODUCTION BY VIRTUAL PHOTONS

Exclusive ϕ production appears within reaction (B). Figure 15 shows the K^+K^- mass distribution for the 4C events fitting reaction (B). A few events are within the experimental resolution (~10 MeV) of the ϕ mass. However, the Chew-Low plot (Fig. 16) reveals that only one event in that region has a reasonably low-momentum transfer and hence a possibility of being a peripherally produced ϕ meson. Within this same region there are 180 ρ's (and 38 ω's). In photoproduction,[13] the ratio of $(\phi \to K^+K^-)$ to $(\rho \to \pi^+\pi^-)$ production is about 1.2% in a comparable W range. If this ratio remained constant at high Q^2, we would have expected to observe 2 $\phi \to K^+K^-$ events. Our observations is statistically consistent with this expectation.

ACKNOWLEDGMENTS

We wish to thank the SLAC operations staff and the engineering and scanning staff of SLAC and of the University of California at Santa Cruz high-energy group for their invaluable contributions to this work. This research was supported in part by the Department of Energy.

APPENDIX A: DENSITY MATRIX ELEMENTS FOR THE ρ MESON

The decay distribution can be written, for the case of an unpolarized lepton beam, in terms of 15 independent decay matrix quantities:

$$
\begin{aligned}
W(\cos\theta, \phi, \phi_\mu) = \frac{3}{4\pi}\{&\tfrac{1}{2}(1 - r^{04}_{00}) + \tfrac{1}{2}(3r^{04}_{00} - 1)\cos^2\theta - \sqrt{2}\,\mathrm{Re}r^{04}_{10}\sin 2\theta\cos\phi - r^{04}_{1-1}\sin^2\theta\cos 2\phi \\
&- \epsilon\cos 2\phi_\mu(r^1_{11}\sin^2\theta + r^1_{00}\cos^2\theta - \sqrt{2}\,\mathrm{Re}r^1_{10}\sin 2\theta\cos\phi - r^1_{1-1}\sin^2\theta\cos 2\phi) \\
&- \epsilon\sin 2\phi_\mu(\sqrt{2}\,\mathrm{Im}r^2_{10}\sin 2\theta\sin\phi + \mathrm{Im}r^2_{1-1}\sin^2\theta\sin 2\phi) \\
&+ [2\epsilon(1+\epsilon)]^{1/2}\cos\phi_\mu(r^5_{11}\sin^2\theta + r^5_{00}\cos^2\theta - \sqrt{2}\,\mathrm{Re}r^5_{10}\sin 2\theta\cos\phi - r^5_{1-1}\sin^2\theta\cos 2\phi) \\
&+ [2\epsilon(1+\epsilon)]^{1/2}\sin\phi_\mu(\sqrt{2}\,\mathrm{Im}r^6_{10}\sin 2\theta\sin\phi + \mathrm{Im}r^6_{1-1}\sin^2\theta\sin 2\phi)\}.
\end{aligned}
$$

The upper index in the matrix elements r_{ij}^{α} refers to the state of virtual-photon polarization ($\alpha = 0, 1, 2$ transverse; $\alpha = 4$ longitudinal; $\alpha = 5, 6$ L-T interference terms). The bottom indices represent the ρ helicity states. Terms of the form r_{ij}^{04} represent the sum of two matrix elements which cannot be separated for fixed W and Q^2 unless the relative contributions from longitudinal and transverse virtual photons are varied (i.e., incident lepton energy).

If $W(\cos\theta, \phi, \phi_\mu)$ is integrated over ϕ and averaged over ϕ_μ one obtains

$$W(\cos\theta) = \tfrac{3}{4}[1 - r_{00}^{04} + (3r_{00}^{04} - 1)\cos^2\theta],$$

so that r_{00}^{04} is the only matrix element affecting $W(\cos\theta)$.

---

*Now at CERN, Geneva, Switzerland.
†Now at Intel Magnetics, Santa Clara, California.
‡Now at Max Planck Institute, Munich, Germany.
§Now at LASL, Los Alamos, New Mexico.
||Now at Commodore Business Machines, Inc., Palo Alto, California.

[1]J. J. Sakurai, Ann. Phys. (N.Y.) 11, 1 (1960). See also J. J. Sakurai, *Currents and Mesons* (University of Chicago Press, Chicago, 1969), and references therein.
[2]J. J. Sakurai and D. Schildknecht, Phys. Lett. 40B, 121 (1972); 41B, 489 (1972); 42B, 216 (1972).
[3]R. P. Feynman, Phys. Rev. Lett. 23, 1415 (1969); see also J. D. Bjorken and E. A. Paschos, Phys. Rev. 185, 1975 (1969).
[4]V. I. Zakharov, in *Proceedings of the XVIII International Conference on High Energy Physics, Tbilisi*, 1976, edited by N. N. Bogolubov *et al.* (JINR, Dubna, U.S.S.R., 1977), Vol. II, p. B69.
[5]See, for example, R. E. Taylor, in *Proceedings of the International Symposium on Lepton and Photon Interactions at High Energies, Stanford, California*, edited by W. T. Kirk (SLAC, Stanford, 1976), p. 679.
[6]G. Knies, Phys. Lett. 27B, 288 (1968).
[7]H. Fraas and D. Schildknecht, Nucl. Phys. B14, 543 (1969).
[8]C. F. Cho and G. J. Gounaris, Phys. Rev. 186, 1619 (1969).
[9]G. Kramer and H. R. Quinn, Nucl. Phys. B55, 222 (1973).
[10]G. Preparata, Phys. Lett. 36B, 53 (1971); M. Sakuraoka, Lett. Nuovo Cimento 3, 89 (1972).
[11]L. N. Hand, Phys. Rev. 129, 1834 (1963).
[12]J. T. Dakin *et al.*, Phys. Rev. D 8, 687 (1973).
[13]J. Ballam *et al.*, Phys. Rev. D 7, 3150 (1973).
[14]ABBHHM collaboration, Phys. Rev. 175, 1669 (1968).
[15]M. Ross and L. Stodolsky, Phys. Rev. 149, 1172 (1966).
[16]P. Söding, Phys. Lett. 19, 702 (1966); A. S. Krass, Phys. Rev. B 159, 1496 (1967).
[17]L. Ahrens *et al.*, Phys. Rev. Lett. 31, 131 (1973).
[18]J. Ballam *et al.*, Phys. Rev. D 10, 765 (1974).
[19]P. Joos *et al.*, Nucl. Phys. B113, 53 (1976).
[20]W. R. Francis *et al.*, Phys. Rev. Lett. 38, 633 (1977).
[21]C. A. Heusch, in *High Energy Physics*, proceedings of the EPS International Conference, Palermo, 1975, edited by A. Zichichi (Editrice Compositori, Bologna, 1976), p. 477; R. F. Mozley, in *Proceedings of the International Symposium on Lepton and Photon Interactions at High Energies, Stanford, California*, 1975, edited by W. T. Kirk (SLAC, Stanford, 1976), p. 783.
[22]G. Wolf, in *Proceedings of the International Symposium on Lepton and Photon Interactions at High Energies*, Stanford, California, 1975, edited by W. T. Kirk (SLAC, Stanford, 1976), p. 795.
[23]P. Joos *et al.*, Nucl. Phys. B122, 365 (1977).
[24]R. Dixon *et al.*, Phys. Rev. Lett. 39, 516 (1977).
[25]C. del Papa *et al.*, Phys. Rev. D 13, 2934 (1976).
[26]S. M. Flatté, C. A. Heusch, and A. Seiden, Nucl. Instrum. Methods 119, 333 (1974).
[27]C. A. Heusch, B. Lieberman, and A. Seiden, Nucl. Instrum. Methods 124, 165 (1975).
[28]Three-view-geometry program, Group A, LBL (unpublished).
[29]APACHE, vertex-finding program, Group A, LBL (unpublished) extensively modified by us.
[30]SQUAW, kinematic-hypothesis-fitting program, Group A, LBL (unpublished).
[31]P. H. Eberhard and W. O. Koellner, Comput. Phys. Commun. 3, 296 (1972).
[32]A phenomenological fit to the MIT-SLAC electroproduction data developed by W. Atwood and S. Stein (private communication).